Transonic Potential Flow Calculations by Two Artificial Density Methods

G. Volpe*
Grumman Corporate Research Center, Bethpage, New York
and
A. Jameson†
Princeton University, Princeton, New Jersey

A steady transonic flow over an airfoil is computed by solving the full potential equation discretized over a contour-fitting grid in full conservation form. Near shock waves, density is corrected to account for the rise in entropy in the region. A multigrid alternating direction method is used to drive the iteration. In supersonic flow regions, artificial dissipation is introduced by retarding the density in the upstream direction. In a new formulation for this artificial density, the amount by which the density is biased is made proportional to the local flux gradients. This new formulation is compared with the standard formulation that is based on density gradients. The new scheme, as the old one, is second-order accurate throughout the flow field except for a small region near shock waves. Results of calculations with the two schemes show that, when the shock itself is weak, the scheme based on flux gradients gives a sharper resolution of the shock than the scheme based on density gradients. As shock strength increases, the shock-capturing abilities of the two schemes become equal. Throughout the range of cases tested, the two schemes exhibited comparable speed and robustness.

Introduction

THE transonic full potential equation is still a very useful and competitive model for describing flow over an airfoil at transonic speeds. Very efficient algorithms have been developed for its solution, in particular by Jameson[1] and Holst.[2] The algorithm devised by Jameson, known as FLO36, has also been coupled with a viscous-interaction method by Melnik and Brook,[3] thus resulting in a widely used tool for computing the viscous transonic flow over airfoils. In all shock-capturing methods, artificial dissipation has to be introduced in regions of supersonic flow to account for the hyperbolicity of the equation there. Dissipation can be added either by addition of an artificial viscosity term as shown in Ref. 1, or by retarding the density as demonstrated in Ref. 4. To enhance the stability of numerical schemes employing one of these forms of artificial dissipation, the second author found that the dissipation had to be activated at a Mach number slightly below one. In addition, second-order-accurate spatial differencing could not be maintained near shock waves. The accuracy of the schemes had to be reduced to first order there. These two factors contributed to smear the shock over some mesh intervals, the number of which depended on the shock strength.

More recently Boerstoel[5] and Hafez et al.[6] have introduced algorithms that use an artificial dissipation based on flux biasing. In these schemes the local density is retarded in the upstream direction an amount that depends on the local flux gradients rather than local density gradients as in the original artificial-density method reported in Ref. 4. For brevity, schemes based on the original artificial-density method will be referred to as density-biasing methods and the newer class of schemes based on flux gradients as flux-biasing schemes, even though they both retard the density. These latter methods follow from a flux-splitting scheme described by Engquist and Osher[7] that specifically rules out expansion shocks. Osher et al.[8] proved this rigorously for two-dimensional flow and also showed that, at least for one-dimensional flow, a compression shock could be captured within one mesh interval. In principle, therefore, it should be possible to get sharper shock definition with flux biasing since there is no need to switch on the artificial dissipation below the sonic Mach number or to reduce spatial accuracy near a shock. The other advantage is that there is no need to define parameters to control when the dissipation is to be activated.

In this paper, a new second-order spatially-accurate artificial-dissipation scheme based on flux biasing is formulated and compared with the standard density-biasing scheme. Except for the dissipation terms, discretization of the full potential equation is otherwise identical in the two methods. The discretized equations are solved via a multigrid alternating-direction (MAD) algorithm first described by Jameson in Ref. 1.

Numerical Method

The equation we seek to solve is the continuity equation

$$\frac{\partial}{\partial x}(\rho u)+\frac{\partial}{\partial y}(\rho v)=0 \tag{1}$$

where x and y are Cartesian coordinates, ρ is the density, and u and v are the two velocity components. Assuming irrotationality, these can be expressed as components of the potential function ϕ

$$u=\phi_x, \qquad v=\phi_y \tag{2}$$

The actual computations are carried out in a region obtained by conformally mapping the exterior of the airfoil in question onto the interior of a circle. A uniform polar coordinate mesh, described by r and θ, then gives an excellent discretization of the flow field. In the mapped plane, the flow equation becomes

$$\frac{\partial}{\partial \theta}(\rho U)+r\frac{\partial}{\partial r}(\rho V)=0 \tag{3}$$

Received July 21, 1986; revision received April 29, 1987.

*Staff Scientist. Member AIAA.

†Professor, Department of Mechanical and Aerospace Engineering.

where

$$U=\phi_\theta, \qquad V=r\phi_r \tag{4}$$

and the physical velocity components in the two coordinate directions are

$$u=\frac{rU}{H}, \qquad v=\frac{rV}{H} \tag{5}$$

where H is the modulus of the transformation to the exterior of the circle.

As described in Ref. 1, at a mesh point i,j in the flow field, Eq. (3) is discretized as

$$\frac{1}{\Delta\theta^2}[\rho_{i+1/2,j}U_{i+1/2,j}-\rho_{i-1/2,j}U_{i-1/2,j}]$$

$$+\frac{r_j}{\Delta r^2}[\rho_{i,j+1/2}V_{i,j+1/2}-\rho_{i,j-1/2}V_{i,j-1/2}]=0 \tag{6}$$

where

$$U_{i+1/,j}=\phi_{i+1,j}-\phi_{i,j} \tag{7a}$$

$$V_{i,j+1/2}=r_{j+1/2}(\phi_{i,j+1}-\phi_{i,j}) \tag{7b}$$

with similar expressions for $U_{i-1/2,j}$ and $V_{i,j-1/2}$. Here $i+1/2$ and $j+1/2$ denote values at midpoints of a mesh interval. The density ρ is computed at cell centers. Hence,

$$\rho_{i+1/2,j}=(1/2)(\rho_{i+1/2,j+1/2}1+\rho_{i+1/2,j-1/2}) \tag{8}$$

At supersonic points, artificial dissipation is introduced by modifying the density in Eq. (6).

Density Biasing

In the standard density biasing scheme formulated by Jameson,[1] at supersonic points the density term ρ in the first bracket in Eq. (6) is replaced by a density that is biased in the upstream direction according to the density gradient; call this $\hat{\rho}$. Thus, assuming the flow to be in the direction of increasing i, we take

$$\hat{\rho}_{i+1/2,j}=\rho_{i+1/2,j}-\mu_{ij}\Delta\theta\left(\frac{\partial\rho}{\partial\theta}\right)_{i,j} \tag{9}$$

A similar expression holds for $\rho_{i-1/2,j}$. Similarly, the density terms in the second bracket of Eq. (6) are replaced by a biased density $\tilde{\rho}$, which is taken to be

$$\tilde{\rho}_{i,j+1/2}=\rho_{i,j+1/2}-\mu_{ij}\Delta r\left(\frac{\partial\rho}{\partial r}\right)_{i,j} \tag{10}$$

$$\mu_{ij}=\text{Max}[0,\ \nu_1(1-M_c^2/M^2)] \tag{11}$$

where M is the local Mach number and $M_c{}^2$ is a user-defined parameter usually less than one, typically 0.9; ν_1 is another user-defined parameter usually set at one. In our scheme, the density is evaluated at each of the cell centers. Thus $(\partial\rho/\partial\theta)_{i,j}$ and $(\partial\rho/\partial r)_{i,j}$ at the mesh point i,j can be evaluated from averaged differences of the densities at the encircling cell centers. Thus, for example,

$$\left(\frac{\partial\rho}{\partial\theta}\right)_{ij}=\frac{1}{2}(\rho_{i+1/2,j+1/2}+\rho_{i+1/2,j-1/2}$$

$$-\rho_{i-1/2,j+1/2}-\rho_{i-1/2,j-1/2}) \tag{12}$$

Application of Eqs. (9) and (10) results in a spatially first-order-accurate scheme in supersonic regions. Second-order accuracy can be recovered by defining

$$\hat{\rho}_{i+1/2,j}=\rho_{i+1/2,j}-\mu_{ij}\Delta\theta\left[\left(\frac{\partial\rho}{\partial\theta}\right)_{i,j}-\epsilon_{ij}\left(\frac{\partial\rho}{\partial\theta}\right)_{i-1,j}\right] \tag{13}$$

and taking $\epsilon_{ij}=1$. The numerical scheme, however, proved unstable unless ϵ_{ij} is made zero near shock waves. A straightforward way of implementing this is to define

$$\epsilon_{ij}=\text{Max}\left(0,\nu_2-\nu_3\left|\Delta\theta\left(\frac{\partial\rho}{\partial\theta}\right)_{ij}+\Delta r\left(\frac{\partial\rho}{\partial r}\right)_{ij}\right|\right) \tag{14}$$

When ν_2 is zero, the scheme is first-order-accurate in supersonic regions. For $\nu_2=1$ partial second-accuracy is introduced. The term ν_3 is a parameter of order one defined by the user. An expression similar to Eq. (13) defines $\tilde{\rho}_{i,j+1/2}$.

Flux Biasing

An alternate method of introducing artificial dissipation in the numerical scheme is by retarding the density based on the flux. This new, alternate scheme follows from the work presented in Refs. 5-8. Thus, in both brackets of Eq. (6) we substitute the density ρ with a retarded density $\hat{\rho}$ defined as

$$\hat{\rho}=\rho-\frac{\Delta s}{q}\frac{\partial F}{\partial s} \tag{15}$$

with

$$F=\rho q \qquad \text{for } M>1$$

$$=\rho^*q^* \qquad \text{for } M\le 1 \tag{16}$$

where q represents total velocity, s represents streamwise direction, and the asterisk denotes sonic conditions. The quantity F, as ρ and q, is evaluated at each cell center. The streamwise gradient is broken up into components in the coordinate directions by

$$\Delta s\frac{\partial F}{\partial s}=\frac{u}{q}\Delta\theta\frac{\partial F}{\partial\theta}+\frac{v}{q}\Delta r\frac{\partial F}{\partial r} \tag{17}$$

In our numerical scheme, this leads to the following representation for the retarded-density terms we define at cell centers:

$$\hat{\rho}_{i+1/2,j+1/2}=\rho_{i+1/2,j+1/2}$$

$$-\left[\left(\frac{u}{q^2}\right)\Delta\theta\left(\frac{\partial F}{\partial\theta}\right)+\left(\frac{v}{q^2}\right)\Delta r\left(\frac{\partial F}{\partial r}\right)\right]_{i+1/2,j+1/2} \tag{18}$$

Second-order-accurate approximations for the gradients in Eq. (18) are given by

$$\Delta\theta\left(\frac{\partial F}{\partial\theta}\right)_{i+1/2,j+1/2}=F_{i+1/2,j+1/2}-F_{i-1/2,j+1/2}$$

$$-\epsilon_{i,j}(F_{i-1/2,j+1/2}-F_{i-3/2,j+1/2}) \tag{19}$$

where ϵ_{ij} is given by Eq. (14). A similar expression holds for $(\partial F/\partial r)_{j+1/2,j+1/2}$.

The obvious advantage of this scheme is that the dissipation is switched on when the local Mach number is unity rather than a smaller subsonic value. The density biasing scheme is not stable with $M_c{}^2=1$.

Entropy Correction

Shocks computed by a potential-flow scheme such as the present one tend to be stronger and, for airfoil flows, are usually located downstream of the location computed by a solution to the Euler equations. Hafez and Lovell[9] devised a method to account for the entropy rise through a shock within the context of a potential formulation. Thus, following Hafez and Lovell, at a mesh point just downstream of a shock, density is multiplied by a factor proportional to the entropy rise through the shock, $\Delta S/R$. For a normal shock and with flow in the direction of increasing i

$$\rho_{i+1/2,j+1/2} \rightarrow \rho_{i+1/2,j+1/2} e^{-\Delta S/S}$$

where

$$\frac{\Delta S}{R} = 2.5\left[\log\left(\frac{7M_1^2-1}{6}\right) - \frac{7}{5}\log\left(\frac{6M_1^2}{M_1^2+5}\right)\right] \tag{20}$$

M_1 is the Mach number computed two points upstream of the shock.

This results in a correction to the residual to the potential equation, as represented by Eq. (6), equal to

$$\Delta\text{Res} = \frac{1}{\Delta\theta}(e^{-\Delta S/R} - 1)\rho_{i+1/2,j} U_{i+1/2,j} \tag{21}$$

Iteration Scheme

The difference equations obtained with either scheme are solved by the MAD algorithm described in Ref. 1. This method employs a multigrid strategy with a generalized alternating-direction method as a smoothing algorithm on each of the meshes. On each mesh, the flow field is alternately swept from the far field toward the airfoil surface and then sequentially along the upper and lower surfaces from leading to trailing edge. With the o-type meshes that we are using, sweep directions follow flow directions reasonably well in supersonic regions. Breakdown of the iteration scheme occurs only when the supersonic region extends all the way to the trailing edge. When this condition does not arise, the method works equally well with either difference scheme.

Results

All the flows to be shown were computed on a 192×32 mesh, and a total of five mesh levels were employed in the multigrid sequence in each case. Each case was computed twice, once employing the flux-biasing scheme and, again, using the density-biasing scheme. The same set of ADI parameters was used for both calculations. In Fig. 1, flow over the NACA0012 airfoil at a freestream Mach number of 0.720 and an angle of attack of 1 deg is depicted as computed by the two schemes. The shock on the upper surface is very weak in this case, as evidenced from the very low drag values, and it is obvious how much better it is resolved by the flux-biasing scheme. As we increase the Mach number and, thus, increase strength of the shock, the shock-capturing capability of the density-biasing scheme as compared to the flux-biasing scheme improves, as we see from Figs. 2 and 3. With a still stronger shock at $M_\infty = 0.75$ and $\alpha = 2$ deg (Fig. 4), we note that the differences between the two schemes become even smaller. In each of these cases the flux-biasing scheme spreads out the jump from supersonic to subsonic conditions over three mesh intervals with most of the jump occurring in the middle one. The smearing with the density-biasing scheme is more substantial with the weaker shocks, but is drastically reduced as the shock strength increases. These observations are also borne out by comparisons of computations for the Korn airfoil at a Mach number of 0.70 for $\alpha = 1$ deg and 2 deg. (Figs. 5 and 6, respectively). The Korn airfoil's design point ($M_\infty = 0.750$, $\alpha = 0$ deg) constitutes a highly sensitive test for a numerical method. The results computed for this case by the two schemes are shown in Fig. 7. The recompression on the upper surface computed with the density-biasing scheme is quite smooth. A sharper recompression is, however, predicted by the flux-biasing method where the shock will form at a higher angle of attack. This is consistent with above-mentioned tendency of the latter scheme to predict sharper recompressions and shocks when these are weak. It should be pointed out that a smooth recompression is obtained with the flux-biasing scheme at an angle of attack of 0.02 deg. As the angle of attack is increased to 0.5 deg (Fig. 8) and to 0.7 deg. (Fig. 9), conclusions similar to the earlier ones are reached. Both schemes could be run throughout the range of applicability of the potential approximation. With only first-order accuracy in the supersonic region ($\nu_2 \equiv 1$), both methods could be made to run until shock reaches the trailing edge as seen in Fig. 10. This case is included only for numerical interest since it is far beyond the physically acceptable limit of our assumptions. Overshoots develop ahead of the shock with both schemes.

	C_L	C_D	C_M
+ + + + FLUX BIASING	0.2038	0.0002	-0.0001
× × × × DENSITY BIASING	0.2038	0.0002	-0.0001

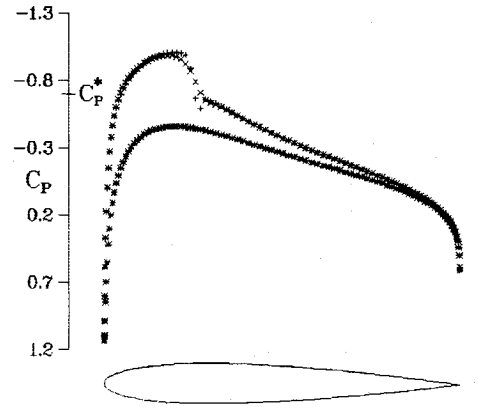

Fig. 1 Pressure distributions computed by flux-biasing and density-biasing schemes, NACA 0012 airfoil ($M_\infty = 0.720$, $\alpha = 1.0$ deg).

	C_L	C_D	C_M
+ + + + FLUX BIASING	0.2122	0.0006	0.0003
× × × × DENSITY BIASING	0.2120	0.0005	0.0003

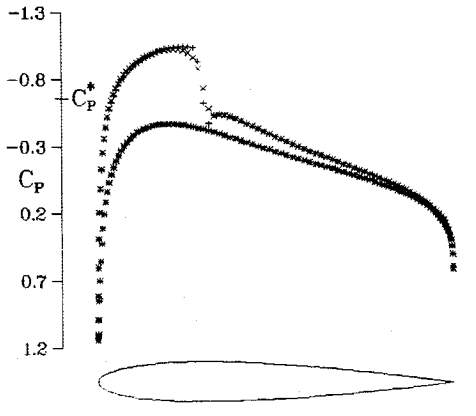

Fig. 2 Pressure distributions computed by flux-biasing and density-biasing schemes, NACA 0012 airfoil ($M_\infty = 0.730$, $\alpha = 1.0$ deg).

	C_L	C_D	C_M
+ + + + FLUX BIASING	0.2366	0.0026	-0.0007
× × × × DENSITY BIASING	0.2357	0.0023	-0.0005

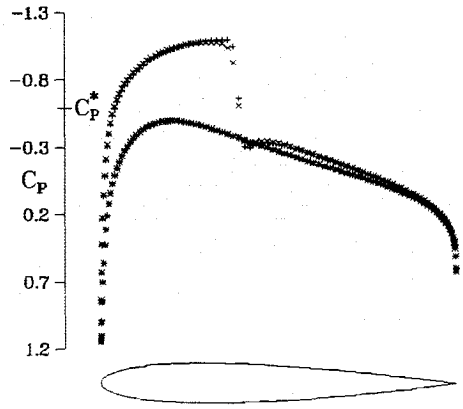

Fig. 3 Pressure distributions computed by flux-biasing and density-biasing schemes, NACA 0012 airfoil ($M_\infty = 0.750$, $\alpha = 1.0$ deg).

	C_L	C_D	C_M
+ + + + FLUX BIASING	0.5130	0.0158	-0.0166
× × × × DENSITY BIASING	0.5094	0.0147	-0.0148

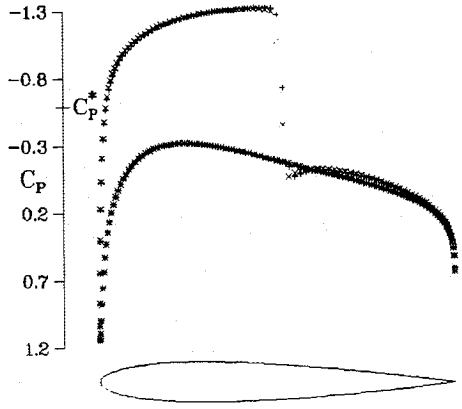

Fig. 4 Pressure distributions computed by flux-biasing and density-biasing schemes, NACA 0012 airfoil ($M_\infty = 0.750$, $\alpha = 2.0$ deg).

	C_L	C_D	C_M
+ + + + FLUX BIASING	0.6986	0.0012	-0.1300
× × × × DENSITY BIASING	0.6980	0.0009	-0.1301

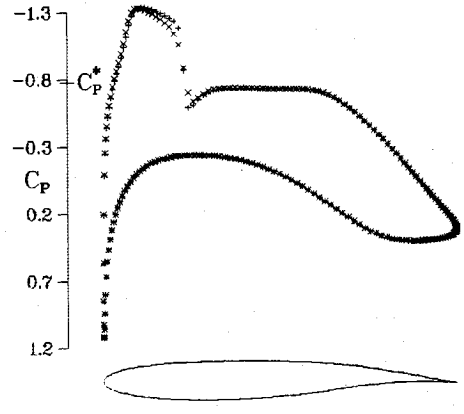

Fig. 5 Pressure distributions computed by flux-biasing and density-biasing schemes, Korn airfoil ($M_\infty = 0.700$, $\alpha = 1.0$ deg).

	C_L	C_D	C_M
+ + + + FLUX BIASING	0.9337	0.0062	-0.1292
× × × × DENSITY BIASING	0.9321	0.0054	-0.1285

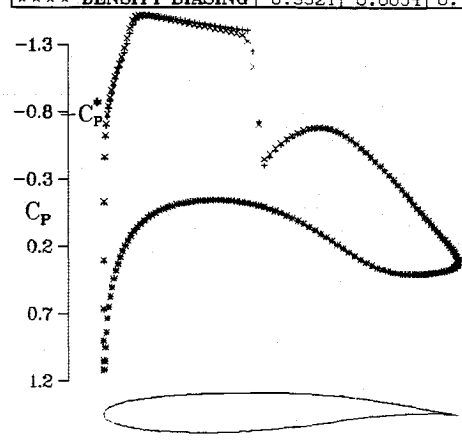

Fig. 6 Pressure distributions computed by flux-biasing and density-biasing schemes, Korn airfoil ($M_\infty = 0.700$, $\alpha = 2.0$ deg).

	C_L	C_D	C_M
+ + + + FLUX BIASING	0.6213	0.0001	-0.1451
× × × × DENSITY BIASING	0.6218	0.0001	-0.1452

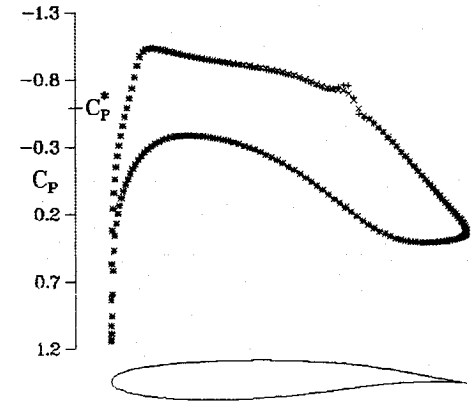

Fig. 7 Pressure distributions computed by flux-biasing and density-biasing schemes, Korn airfoil ($M_\infty = 0.750$, $\alpha = 0$ deg).

	C_L	C_D	C_M
+ + + + FLUX BIASING	0.6512	0.0003	-0.1474
× × × × DENSITY BIASING	0.6520	0.0006	-0.1493

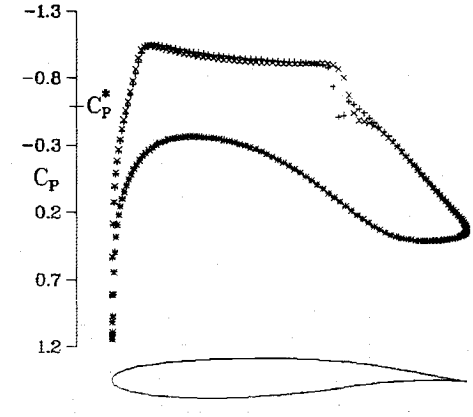

Fig. 8 Pressure distributions computed by flux-biasing and density-biasing schemes, Korn airfoil ($M_\infty = 0.750$, $\alpha = 0.2$ deg).

	C_L	C_D	C_M
+ + + + FLUX BIASING	0.8279	0.0072	-0.1712
× × × × DENSITY BIASING	0.8283	0.0068	-0.1711

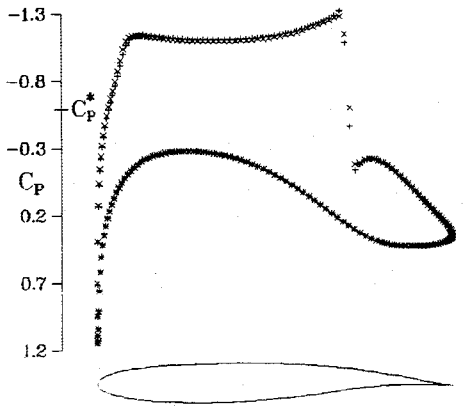

Fig. 9 Pressure distributions computed by flux-biasing and density-biasing schemes, Korn airfoil ($M_\infty = 0.750$, $\alpha = 0.7$ deg).

	C_L	C_D	C_M
+ + + + FLUX BIASING	1.3084	0.0941	-0.4388
× × × × DENSITY BIASING	1.3192	0.0939	-0.4416

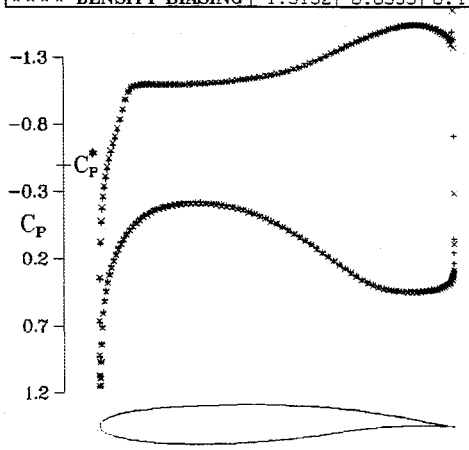

Fig. 10 Pressure distributions computed by flux-biasing and density-biasing schemes, Korn airfoil ($M_\infty = 0.780$, $\alpha = 0.9$ deg).

Table 1 Cycles required for convergence

Airfoil	M_∞	α, deg	Flux biasing	Density biasing
NACA 0012	0.720	1.0	19	13
NACA 0012	0.730	1.0	17	15
NACA 0012	0.750	1.0	19	24
NACA 0012	0.750	2.0	59	55
Korn airfoil	0.700	1.0	25	18
Korn airfoil	0.700	2.0	43	43
Korn airfoil	0.750	0.0	128	39
Korn airfoil	0.750	0.2	39	41
Korn airfoil	0.750	0.7	108	95
Korn airfoil	0.780	0.9	138	260

Table 1 gives the number of cycles needed to obtain convergence, defined as attainment of an average residual of 5.0×10^{-8}. In most cases, the density-biasing scheme is marginally faster. The flux-biasing scheme shows a substantial advantage only in the last example. As mentioned above, runs were made with the same set of ADI parameters for both dissipation schemes. It is possible that convergence might be speeded up for either scheme with different parameters.

Concluding Remarks

A new second-order-accurate form of artificial dissipation based on flux biasing has been introduced and compared with the standard form based on density biasing using an otherwise identical numerical method for computing the steady transonic flow over an airfoil. The numerical experiments have shown that the new scheme is as robust as the old one and has similar convergence qualities. For weak shock waves, the flux-biasing scheme gives a sharper definition of a shock than the density-biasing scheme. In all cases, the former scheme captures most of the jump in one mesh interval and all of it within three intervals. The density-biasing scheme shock-capturing ability improves with increasing shock strength and equals that of the new scheme for strong shock waves. The more extensive smearing of the older density-biasing scheme is, apparently, due to the need to switch on the dissipation at a Mach number lower than one to enhance stability. As the shock strength increases, the number of subsonic points at which dissipation is turned on decreases. This is a possible explanation for improvement in shock prediction vis-à-vis the flux-biasing scheme. The most attractive feature of the flux-biasing method is, of course, that the dissipation is needed only at supersonic points.

References

[1]Jameson, A., "Acceleration of Transonic Potential Flow Calculations on Arbitrary Meshes by the Multiple Grid Method," AIAA Paper 79-1458, 1979.

[2]Holst, T., "Implicit Algorithm for the Conservative Transonic Full Potential Equation Using an Arbitrary Mesh," *AIAA Journal*, Vol. 17, Oct. 1979, pp. 1038–1045.

[3]Melnik, R.E. and Brook, J.W., "The Computation of Viscid/Inviscid Interaction on Airfoils with Separated Flow," presented at Third Symposium on Numerical and Physical Aspects of Aerodynamic Flows, California State Univ., Jan. 1985.

[4]Hafez, M.M., Murman, E.M., and South, J.E., "Artificial Compressibility Methods for Numerical Solution of Transonic Full Potential Equation," AIAA Paper 78-1148, 1978.

[5]Boerstoel, J.W., "A Multigrid Algorithm for Steady Transonic Potential Flows Around Airfoils Using Newton's Iteration," *Journal of Computational Physics*, Vol. 48, 1982, pp. 313–343.

[6]Hafez, M.M., Osher, S., and Whitlow, W., "Improved Finite Difference Schemes for Transonic Potential Calculations," AIAA Paper 84-0092, 1984.

[7]Engquist, B. and Osher, S., "Stable and Entropy Satisfying Approximations for Transonic Flow Calculations, *Mathematics of Computation*, Vol. 34, No. 149, 1980, pp. 45–75.

[8]Osher, S., Hafez, M., and Whitlow, W., "Entropy Condition Satisfying Approximations for the Full Potential Equation of Transonic Flow," *Mathematics of Computation*, Vol. 44, No. 169, 1985, pp. 1–29.

[9]Hafez, M. and Lovell, D., "Entropy and Vorticity Corrections for Transonic Flows," AIAA Paper 83-1926, 1983.